

<https://doi.org/10.1038/s41524-025-01593-7>

Nanoscale confinement of phonon flow and heat transport

Check for updates

Albert Beardo^{1,2}✉, Weinan Chen^{3,4}, Brendan McBennett¹, Tara Karimzadeh Sabet³, Emma E. Nelson¹, Theodore H. Culman¹, Henry C. Kapteyn^{1,5}, Joshua L. Knobloch^{1,6}, Margaret M. Murnane¹ & Ismaila Dabo³

Efficient thermal management is critical to device performance and reliability for energy conversion, nanoelectronics, and the development of quantum technologies. The commonly-used diffusive model of heat transport breaks down for confined nanoscale geometries, and advanced theories beyond diffusion are based on disparate assumptions that lead to conflicting predictions. Here, we outline and contrast the two predominant formulations of the Boltzmann equation for heat transport in semiconductors, namely, the ballistic and hydrodynamic models. We examine these methods in light of experiments and atomistic calculations of heat fluxes and temperature profiles in phononic systems with nanometer-sized features. We argue that reconciling the hydrodynamic and ballistic formulations is an outstanding necessity to develop a unifying theory of confinement effects on phonon flow, which will ultimately lead to optimal strategies for thermal management in nanodevices.

The efficiency and durability of energy conversion systems and data-processing devices critically depend on effective thermal management, since operating temperatures significantly influence functionality and intrinsic properties, and can modify energy flow. To push electric vehicles to higher performance or to enable higher-speed communications, transistors with higher power and higher frequencies are required¹. However, in power transistors based on wide-bandgap materials, hot spots can form at buried interfaces. These can have dimensions of tens of nanometers and can limit device performance and lifetime to an extent not captured by diffusion-based heat transport models^{1,2}. Such thermal roadblocks exist not only in emerging devices but also in current technologies—clock-speeds of modern processors have not significantly increased since the early 2000s due to high heat loads³. Mitigating these effects is challenging; there is no widely accepted model of heat flow that is sufficiently tractable computationally to be applied to technologically relevant geometries, with complex three-dimensional designs incorporating multiple materials and spanning multiple length scales.

It is well-established that Fourier's law of heat diffusion along macroscopic thermal gradients breaks down at length and frequency scales comparable to the mean free paths (MFPs) and scattering rates of the microscopic energy carriers, namely, the phonons in semiconductors such as silicon^{4,5}. Under complex non-equilibrium conditions, the diffusive model cannot reproduce experimental observations, even in an effective form with adjustable thermal conductivity or interface resistance

parameters^{6,7}. Predominant models developed for highly confined geometries that go beyond diffusion often produce disparate behaviors; some predict ray-like phonon transport reminiscent of light propagation (the Casimir model)^{8–10}, while others predict phonon flow which conforms to the boundaries in analogy to fluid dynamics^{11,12}. While there is some consensus that such non-diffusive phonon behaviors appear at cryogenic temperatures and low-dimensional materials, there is still much debate about their relevance in room-temperature devices and nanoscale structures. Clearly, advanced thermal management strategies leveraging ray-like optical analogies would differ significantly from strategies derived from hydrodynamic fluid dynamics. Thus, further investigation of highly confined heat flow is crucial for optimizing energy-conversion and nanoelectronic devices.

Boltzmann transport

Advanced models of heat conduction start from the Boltzmann transport equation (BTE) for phonons,

$$\frac{\partial f_\lambda}{\partial t} + \vec{v}_\lambda \cdot \vec{\nabla} f_\lambda = C(f_\lambda), \quad (1)$$

where f_λ is the phonon distribution function of the λ -phonon mode (here, λ stands for the wave-vector \vec{k} and polarization s), \vec{v}_λ is the phonon group velocity, and C is the linearized collision operator. Equation (1) is a particle-like description of phonon transport that neglects any coherent behavior

¹Department of Physics, JILA, and STROBE NSF Science and Technology Center, University of Colorado and NIST, Boulder, CO, USA. ²Department of Physics, Universitat Autònoma de Barcelona, Bellaterra, Catalonia, Spain. ³Department of Materials Science and Engineering and Wilton E. Scott Institute for Energy Innovation, Carnegie Mellon University, Pittsburgh, PA, USA. ⁴Application Engineering, MathWorks, Natick, MA, USA. ⁵KMLabs Inc., Boulder, CO, USA.

⁶Department of Physics, Utah State University, Logan, UT, USA. ✉e-mail: albert.beardo@uab.cat

that might emerge at low temperatures or in sufficiently confined situations^{13,14}. The development of density functional theory^{15,16} cleared the way for the ab initio determination of the operator C in bulk conditions^{17,18}, thus enabling the calculation of the bulk thermal conductivity for a wide range of crystalline materials via iterative methods¹⁷ or the relaxon approach¹⁹. However, the need to incorporate complex boundary conditions and transient energy sources prevents the solution of the full linearized BTE in all but a few idealized nanoscale geometries^{20,21}.

Over the last decades, significant effort has been devoted to both simplifying and implementing Eq. (1) beyond bulk conditions, i.e., for non-homogeneous or rapidly varying thermal fields, and in the presence of boundaries. These methods can be classified into two main categories: the ballistic (Casimir) interpretation^{8,22–25}, consisting of direct solutions of Eq. (1) with a simplified form of the operator C, and the moment-based, or hydrodynamic, interpretation^{11,26–28}, formulated upon projections of Eq. (1) into a reduced set of statistical moments of the distribution function. The former approach generally assumes that the coupling between phonon modes can be embodied in a single mode-dependent relaxation time that is independent of the non-equilibrium state, and that each mode interacts independently with system boundaries. In principle, this description provides full knowledge of the phonon distribution f_λ , which can then be locally related with macroscopic magnitudes such as the temperature field or the heat flux distribution. In contrast, the hydrodynamic approach does not necessarily require any simplification of the operator C, and thus inherently accounts for collective phonon evolution, or inter-mode coupling. It instead simplifies the distribution function by solving for it within a sub-space determined only by its lowest-order statistical moments, which are explicitly related to the temperature and heat flux variables. This simplification enables reconciling the treatment of the linearized BTE with non-equilibrium thermodynamic considerations such as the positive production of entropy^{29,30}. However, it prevents its general applicability to arbitrarily complex non-equilibrium conditions at length or time scales much smaller than the phonon mean free paths and scattering times.

In this perspective, we compare the ballistic and hydrodynamic interpretations of nanoscale heat conduction in paradigmatic non-equilibrium conditions, where the phonon flow is highly constrained in nanostructured silicon. First, we highlight the similarities and fundamental differences underlying the two approaches, including single- and multi-scale deviations from bulk diffusive transport and differing treatments of phonon-boundary scattering. Then, we present the respective predictions of the local heat flux and temperature distributions in a phononic crystal geometry, and their relation to experimental observables such as the apparent conductivity. We compare these results to non-equilibrium molecular dynamics simulations in the same system. We conclude by establishing analogies with nanoscale electron transport and discussing experiments and hypotheses that may reconcile these approaches to modeling thermal transport.

Ballistic framework

The complexity of the BTE can be significantly reduced via the relaxation time approximation (RTA),

$$C(f_\lambda) = -\frac{f_\lambda - f_\lambda^{\text{eq}}}{\tau_\lambda}, \quad (2)$$

where τ_λ is the characteristic relaxation time of mode λ , embodying all potential phonon scattering processes, which are treated as independent events. The scattering rates can be evaluated ab initio using density functional theory in bulk crystals¹⁸, leaving no adjustable parameters. Within the RTA framework, macroscopic variables like the thermal conductivity κ can be expressed in terms of the additive contribution of the phonon modes,

$$\kappa = \frac{1}{3} \int v_\lambda^2 c_\lambda \tau_\lambda d\lambda, \quad (3)$$

where c_λ is the phonon-resolved specific heat capacity.

When extrapolating this framework to nanostructured systems, it is necessary to further assume that each phonon mode interacts independently with the system boundaries. Following an optical analogy, the probability of a specular or diffuse boundary scattering event depends only on the wavelength of the phonons and the surface roughness³¹. This approach has been used to model and interpret a variety of recent measurements of heat flow at the nanoscale^{9,10,32}, and has promoted the development of multiple deterministic^{10,33,34} and stochastic^{9,35,36} algorithms to simulate phonon dynamics in complex structures including two- and three-dimensional phononic crystals. In Box 1, we provide a representative implementation of this framework for arbitrary nanoscale geometries.

Intuitive insight on the ballistic picture is accessible through the notions of phonon suppression²⁴, cumulative thermal conductivity¹⁸, MFP spectroscopy³⁷, and Lévy flights³⁸. In system geometries presenting a single characteristic length scale L , such as a thin film or a sinusoidal thermal pattern, it has been proposed that the apparent conductivity of the system is the cumulative contribution in Eq. (3) of the phonon-modes with mean free path smaller than $L^{37,39}$. As shown in Fig. 1a, the cumulative conductivity according to the ab initio relaxation time spectrum in room-temperature silicon predicts that the reduction of the conductivity by reducing system size occurs smoothly over multiple orders of magnitude, from the few micron to the few nanometer scales, thus suggesting that phonon transport at the nanoscale is inherently a multi-scale phenomenon. This implies a reduction in thermal conductivity at length scales much larger than the average mean free path $\bar{\Lambda}$.

Hydrodynamic framework

In contrast to the ballistic framework, which solves the linearized BTE (Eq. (1)) in terms of the phonon mode populations, the hydrodynamic approach expresses the evolution of f_λ in terms of its statistical moments²⁶. In principle, any solution of the BTE can be equivalently expressed in the basis of statistical moments. However, for practical reasons, only the projections of Eq. (1) into the lowest order moments are considered. This underlying assumption is usually justified via a variational principle³¹. The intuitive picture is that scattering mechanisms rapidly reduce the statistical complexity of the distribution function (i.e., relax the high order moments) due to entropy maximization, and only the lowest statistical moments are required to properly characterize the non-equilibrium state²⁸. The moment projections of the BTE result in mesoscopic equations in terms of the temperature T and the heat flux \vec{q} , which can be formulated as a hydrodynamic heat equation⁴⁰,

$$\tau \frac{\partial \vec{q}}{\partial t} + \vec{q} = -\kappa_{\text{GK}} \vec{\nabla} T + \ell^2 (\vec{\nabla}^2 \vec{q} + \alpha \vec{\nabla} \vec{\nabla} \cdot \vec{q}), \quad (4)$$

where τ , κ_{GK} , ℓ , and α are the flux relaxation time, the bulk thermal conductivity, the non-local length, and a dimensionless viscosity coefficient, respectively. These parameters are intrinsic properties corresponding to specific averages over the phonon population²⁸. Equation (4) generalizes Fourier's law by incorporating memory and non-local effects, which become relevant at characteristic length and time scales representative of the collective relaxation of the main non-equilibrium feature of the distribution, i.e., the heat flux. This formulation inherently describes the phonon evolution as a collective phenomena, where the thermodynamic laws are implicitly accounted for⁴¹. This results in the prediction of non-diffusive effects that are incompatible with the ballistic approach, such as second sound in rapidly varying temperature fields or Poiseuille flow in the presence of boundaries. Interestingly, the hydrodynamic model equations are instead closely related to alternative mesoscopic approaches such as the dual-phase lag model⁴² and non-equilibrium thermodynamic formalisms³⁰.

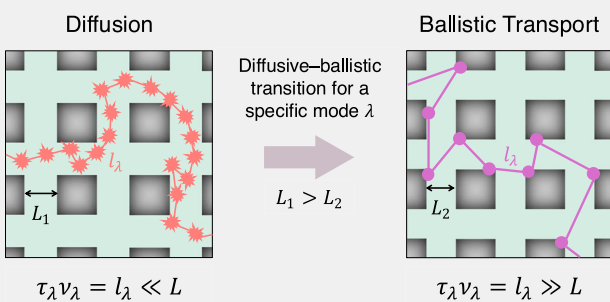
A variety of numerical methods, including finite elements, can be used to seek solutions to the hydrodynamic transport equation^{43,44}, and the input coefficients κ_{GK} , ℓ , τ , and α can be obtained from ab initio calculations²⁸, as extensively used to model a variety of experiments^{7,11,45,46}. Instead of modeling the interaction of the boundaries with each phonon mode individually,

Box 1 | Ballistic framework

The steady-state evolution of each phonon mode λ is effectively decoupled from the other modes and is governed by the BTE under RTA:

$$\vec{v}_\lambda \cdot \nabla f_\lambda = -\frac{f_\lambda - f_\lambda^{\text{eq}}}{\tau_\lambda}.$$

In response to an **arbitrary thermal perturbation**, crystal anharmonicity induces scattering within the phonon population and with defects and relaxes the population of each mode back to local equilibrium at a rate characterized by the mode-dependent relaxation time τ_λ . In the simplest picture, the phonon momentum is destroyed upon collision with boundaries and asperities, and the propagation direction is randomized. Thus, the emitted phonons from the boundaries are assumed to follow an equilibrium distribution at a temperature determined by the stationary local equilibrium.



Within the Casimir interpretation, in **highly confined nanochannels** with characteristic size L smaller than most of the MFPs $\tau_\lambda v_\lambda = l_\lambda$, phonons travel ballistically between boundaries and stochastically percolate through the system.

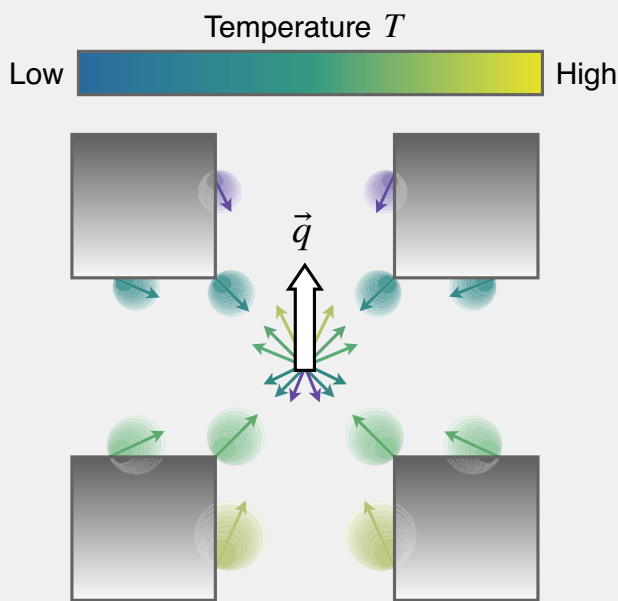
Under **confinement**, some modes have a MFP l_λ smaller than the system size L and some have l_λ larger than L . The former experience internal scattering and diffuses through the system from hot to cold while the latter evolves via ballistic transport, thus only changing direction upon collision with a boundary.

In both confined and highly confined conditions, the local heat flux in a given point can be calculated by integrating the emitted flux from all the geometrically accessible boundaries. If the temperature of the

boundaries is not homogeneous, the heat flux is not balanced and an energy current is established. For diffusive modes ($l_\lambda \ll L$), intrinsic scattering randomizes the phonon propagation direction and exponentially attenuates their heat flux contribution:

$$\bar{q}(\vec{r}) \propto \sum_\lambda \int_S e^{-|\vec{r}-\vec{r}'|/l_\lambda} f_\lambda^{\text{eq}}(\vec{r}') h\omega_\lambda \vec{v}_\lambda \frac{d\Omega'}{4\pi},$$

where ω_λ is the phonon frequency and the integral is performed over the surface area of the **accessible boundaries** from point \vec{r} . The temperature determining f_λ^{eq} of the emitted phonons in boundary locations \vec{r}' is initially prescribed as a linear decay from hot to cold terminals and then can be iteratively calculated to ensure energy balance in all boundaries.

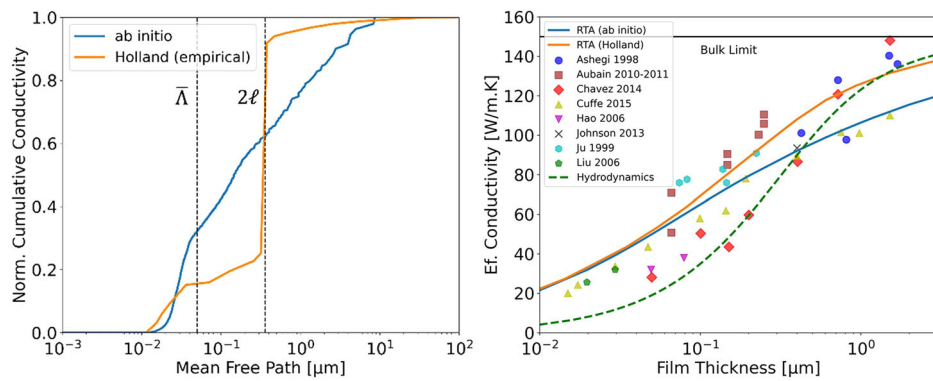


For length scales larger than all the mean free paths, Casimir's model recovers Fourier's law with a conductivity described by Eq. (3).

Fig. 1 | Onset of nanoscale heat transport effects.

a Relative cumulative thermal conductivity in silicon at 300 K as a function of phonon mean free path according to the phenomenological Holland model³⁹ and the ab initio calculated spectrum. The average of the phonon mean free path weighted by the specific heat $\bar{\Lambda}$, and the hydrodynamic characteristic length 2ℓ are shown as vertical lines.

b Effective in-plane thermal conductivity in silicon films as a function of thickness. A selection of experiments^{4,39,72–78} is compared to ballistic predictions with the ab initio and Holland spectrums, respectively, along with hydrodynamic solutions using ab initio calculated parameters $\kappa_{\text{GK}}=150$ W/(m · K) and $\ell = 180$ nm. All models assume fully diffuse phonon-boundary scattering.



Box 2 | Hydrodynamic framework

Under nanoscale confinement in steady state, the deviation from the equilibrium phonon distribution function is assumed to be solely dependent on the heat flux and the heat flux gradient:

$$\mathbf{f}_\lambda = \mathbf{f}_\lambda^{\text{eq}} + \vec{\beta}_\lambda \cdot \vec{\mathbf{q}} + \vec{\mathbf{G}}_\lambda : \vec{\nabla} \vec{\mathbf{q}},$$

where $\vec{\beta}_\lambda$ and $\vec{\mathbf{G}}_\lambda$ are vectorial and tensorial weights that can be determined by solving the BTE. Any type of phonon interaction is implicitly assumed to rapidly and efficiently relax the higher-order perturbations.

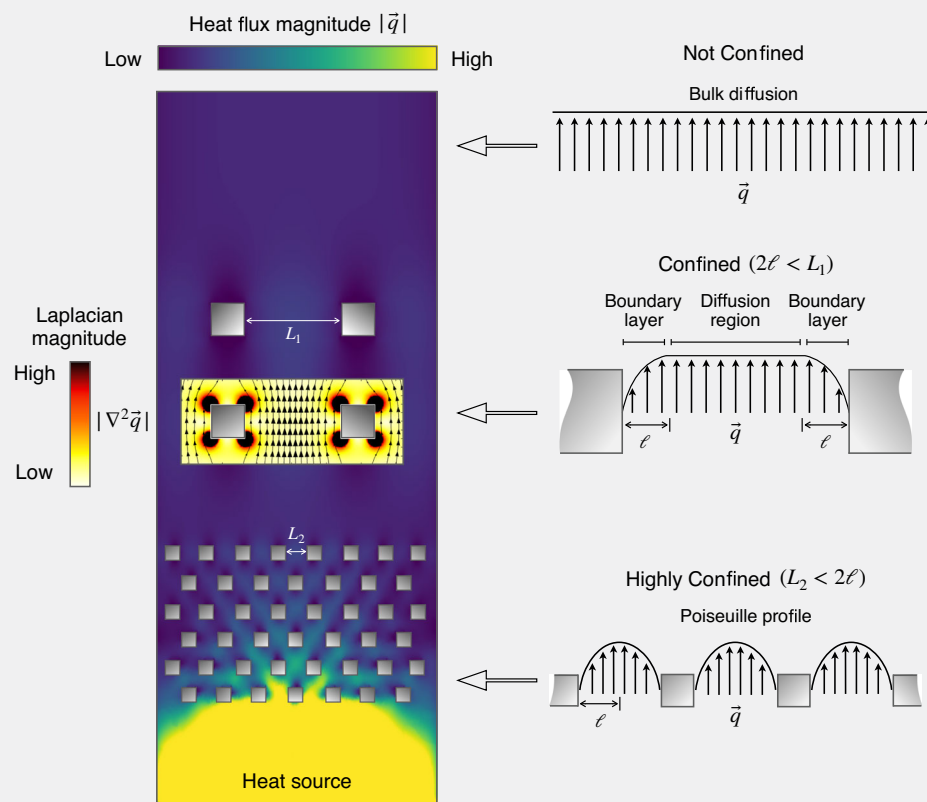
As obtained by projecting Eq. (1), this distribution implies a hydrodynamic equation, along with energy conservation and slip boundary

conditions:

$$\vec{\mathbf{q}} = -\kappa_{\text{GK}} \vec{\nabla} \mathbf{T} + \ell^2 \vec{\nabla}^2 \vec{\mathbf{q}}, \quad \vec{\nabla} \cdot \vec{\mathbf{q}} = 0,$$

$$\vec{\mathbf{q}} \cdot \vec{n} = 0, \quad \mathbf{q}_t = -\mathbf{C} \ell \vec{\nabla} \mathbf{q}_t \cdot \vec{n},$$

where \vec{n} is the boundary-normal vector and t denotes tangential component. The conductivity κ_{GK} and the non-local length ℓ are integrals over λ of $\vec{\beta}_\lambda$, $\vec{\mathbf{G}}_\lambda$, and the slip length $C\ell$ depends on surface roughness.



For **arbitrary thermal perturbations** at the nanometer scale, the assumed simplification for the distribution does not accommodate sufficient complexity, and the governing mesoscopic transport equation is unknown.

The evacuation of heat through **highly confined nanochannels** (sizes L smaller than 2ℓ) involves a severely constrained phase space for phonon evolution, wherein the ansatz for f_λ is incomplete. The hydrodynamic equation in effective form can be used to approximate inhomogeneous flux profiles and nanoscale effects in terms of hydrodynamic analogs.

Under **confinement** (sizes L larger than 2ℓ) the ansatz for f_λ is appropriate, and the hydrodynamic equation with intrinsic parameter values can be used to predict the heat flux profiles and the apparent conductivity. In analogy to slip flow and boundary layers in rarefied fluids, a reduction of $\vec{\mathbf{q}}$ is predicted in regions where $\vec{\nabla}^2 \vec{\mathbf{q}} > 0$ due to boundaries, obstacles, and inhomogeneous temperature gradients.

For wider heat evacuation channels, the deviation from equilibrium is proportional to $\vec{\mathbf{q}}$, which is uniform, and the hydrodynamic equation reduces to Fourier's law.

the boundary conditions are imposed at the level of the integrated magnitudes T and \vec{q} , allowing for simple implementation even in complex geometries and interfaces. In Box 2, we present a summary of the key assumptions underlying the hydrodynamic model and illustration of its implementation in steady-state conditions (examples of the general implementation for transient experiments can be found elsewhere^{7,47,48}).

Heat flow that follows a hydrodynamic-like transport equation, such as Eq. (4), has been a long-standing prediction since the early work of Guyer, Krumhansl, and others^{40,49–51}; however, while this behavior has been traditionally considered exotic, only occurring within a narrow range of materials and temperatures, recent theoretical and experimental works suggest that hydrodynamic effects generally emerge at the nanoscale in crystalline

semiconductors^{11,28}. Specifically, the applicability of the hydrodynamic framework to describe phonon transport was originally assumed to be restricted to extremely low temperatures, where momentum-conserving (normal) scattering events are more frequent than the resistive ones. In this regime, known as the Ziman (collective) limit, the abundance of inter-mode transitions that do not relax the distribution back to equilibrium induces a phonon drift, thus microscopically justifying hydrodynamic effects⁴⁹. More recently, two-dimensional materials like graphene were predicted to sustain the Ziman limit at higher temperatures^{52,53}, and experiments confirmed the emergence of hydrodynamic phonon behavior in the collective regime^{54,55}. The microscopic criteria for the emergence of hydrodynamic transport, however, are under debate. According to the moment-based treatment of the BTE, Eq. (4) can be derived without assuming the dominance of normal collisions^{11,28}. Consistently, a variety of experiments displaying non-diffusive behavior in 3D semiconductors at high temperatures have been predicted using the hydrodynamic description^{7,28,46}. Moreover, recent ab initio investigations on the role of four-phonon processes indicate that the dominance of normal collisions in materials like graphene is not as important as previously thought, even in bulk conditions⁵⁶. These recent advances suggest that Eq. (4) is the natural generalization of Fourier's law in general semiconductors in constrained situations, such as complex silicon or germanium nanostructures, or under the influence of rapidly varying energy sources. The dominance of normal collisions according to ab initio calculations (i.e., assuming a bulk crystal) thus seems a sufficient but not necessary condition for the emergence of hydrodynamic behavior. Instead, the scarcity of resistive collisions at the nanoscale prevents rapid homogenization of the heat flux distribution, invoking inter-mode correlations and collective phonon evolution enforced by thermodynamic constraints, such as energy conservation and entropy production optimization, that are typically negligible when calculating bulk conductivity near equilibrium.

The generalized hydrodynamic approach for nanoscale heat flow, however, cannot model situations where the non-equilibrium situation is arbitrarily complex and the phonon distribution varies arbitrarily rapidly in time and space²⁶, as higher-order terms in the moment expansion of the distribution function become more relevant. The general applicability of Eq. (4) has not been demonstrated for Knudsen number $\text{Kn} = \ell/L$ larger than one, where L is the smallest characteristic scale of the system⁴⁴. Nonetheless, effective hydrodynamic approaches with modified versions of the intrinsic parameters have still shown applicability beyond the traditional bounds of ab initio predictability¹², as discussed further in the following section.

Implications of the ballistic and hydrodynamic pictures

Although both the ballistic and hydrodynamic approaches are based on the phonon gas model and the linearized BTE (Eq. (1)), they are challenging to reconcile. A key difference is their respective prediction of a multi- or single-scale onset of nanoscale effects, i.e., deviations from bulk diffusion, in confined systems⁴⁵. Figure 1b plots the room-temperature effective thermal conductivity κ of a silicon thin film as a function of its thickness L using the hydrodynamic and ballistic models. From the analytic solution of the hydrodynamic equation with slip boundary conditions in the thin film⁵⁷, one obtains

$$\kappa = \kappa_{\text{GK}} \left(1 - \frac{2 \text{Kn} \tanh(\text{Kn}^{-1}/2)}{1 + C \tanh(\text{Kn}^{-1}/2)} \right), \quad (5)$$

where $\text{Kn} = \ell/L$, and the slip coefficient C is set to 1 for fully diffuse boundaries^{31,44}. Accordingly, a rapid decline in thermal conductivity is predicted at film thickness around 300–400 nm, which corresponds to twice the non-local length ℓ in silicon of 180 nm at 300 K²⁸. The fact that the heat flux relaxation scale ℓ is larger than the average mean free path weighted by the specific heat $\bar{\Lambda} \sim 50$ nm explains the emergence of nanoscale effects at scales of hundreds of nanometers without invoking the notion of multiscale phonon transport⁵⁸. Conversely, instead of a sudden onset of non-Fourier phenomena at a characteristic length scale, the ballistic model predicts a gradual manifestation of nanoscale effects starting at length scales equal to

the longest mean free paths of the heat-carrying phonons, wherein a fraction of the phonon spectrum behaves ballistically and the rest diffusively^{22,24}. This behavior has been associated with superdiffusion and Lévy flights³⁸, and experimentally validated in alloys^{59–61}. In pure semiconductors such as silicon, these effects have also been suggested as a direct consequence of the independent evolution of the phonon modes assumed by the RTA, combined with the multi-scale mean free path spectrum obtained from ab initio calculations¹⁸. Figure 1a illustrates this broad spectrum appearing as a smooth increase in spectral thermal conductivity over multiple orders of magnitude. Accordingly, nanoscale effects are predicted to arise even at 10 μm length scales.

Within the ballistic framework, the bulk ab initio mean free path spectrum is not the only input spectrum currently being used to model experiments. Alternatively, a phenomenological fit of the bulk conductivity, known as the Holland spectrum^{39,62}, is still being used to interpret experiments in nanoscale silicon systems such as nanowires or phononic crystals^{63,64}. Although the Holland model was not inspired by collective phonon effects, it displays a sharp decay of the cumulative conductivity at a particular length scale around 2ℓ . Remarkably, since this is the size of the boundary layers where non-Fourier effects manifest according to Eq. (4), the ballistic model with the Holland spectrum predicts a similar onset of nanoscale effects as the hydrodynamic description (see Fig. 1).

Further differences between the two interpretations can be identified in terms of the respective model applicabilities. For example, Fig. 1b illustrates an evident limitation of the hydrodynamic approach. For very large Knudsen numbers $\text{Kn} \gg 1$, the hydrodynamic model with ab initio parameters clearly underestimates the effective conductivity of the films⁴⁴. This is associated with the limitations of the moment method in extremely confined conditions, where the expansion of the distribution on the lowest order moments may be insufficient⁶⁵. In such cases, it is under debate whether the hydrodynamic description still holds, or whether the different phonon modes become effectively uncorrelated and ballistic dynamics appear. Previous work suggests that effective modeling is still possible for large Knudsen numbers with parameters in Eq. (4) characterized experimentally^{12,66} or fitted to molecular dynamics simulations⁶⁷. Microscopically, this would imply phonon scattering and momentum diffusion in highly confined environments ($\text{Kn} \gg 1$) occur at length scales smaller than the ab initio non-local length, which is calculated using density functional theory, i.e., considering the phonon dispersion and force constants in infinitely periodic crystals. Hence, reconciling ab initio calculations with the hydrodynamic approach in extremely confined situations is still an open question.

In the ballistic framework, on the other hand, it is recognized that neglecting the inter-mode transitions as per Eq. (2) can inject unphysical features in the modeling. One paradigmatic example is the violation of energy conservation⁶⁸, which can be addressed in the RTA picture by considering deviational energy formulations of Eq. (1)^{35,38}, or by introducing a notion of pseudo-equilibrium temperature²⁰. Additionally, the RTA neglects the emergence of collective effects^{40,69}, potentially arising in the presence of normal collisions or in constrained phase spaces during phonon evolution at the nanoscale. Indeed, the suitability of the RTA is often justified in terms of thermal conductivity predictions in bulk conditions. In materials like silicon or germanium at non-cryogenic temperatures, where normal collisions are present but not dominant, Eq. (3) reproduces the bulk conductivity obtained from iterative methods and experiments with reasonable accuracy. Consistently, Callaway's approximation to model the role of normal collisions in the bulk induces only a small correction for these materials⁶⁹. However, while accounting for intermode coupling is not critical to describe the bulk behavior in standard semiconductors, this does not necessarily imply that this approach with ab initio (bulk) phonon properties can be extrapolated to model nanoscale effects in the same materials^{70,71}.

Inspecting phonon flow in silicon phononic crystals

As discussed above, the ballistic and hydrodynamic models display some features that are not easily reconcilable from a theoretical point of view, such

as the amount of relevant degrees of freedom for f_λ and the number of intrinsic phonon length scales required in each respective description. However, as illustrated in Fig. 1b, comparing global metrics, such as the apparent thermal conductivity and its deviation from bulk diffusion, to experimental measurements^{4,39,72–78} is usually insufficient to discriminate between the models. Therefore, analysis of local magnitudes under well-defined confinement situations is necessary to clarify the nature of phonon transport at the nanoscale and establish revised criteria for the applicability of each model.

To this end, three-dimensional phononic crystals provide a telling case of study. Recent experiments in this specific geometry have been modeled using both the ballistic and hydrodynamic frameworks in refs. 10,12, respectively. While these models provide an interpretation of the global behavior, the underlying physics and local predictions according to each model are not necessarily in agreement. Here, we consider a phononic crystal consisting of crystalline silicon interrupted by periodically arranged cubic empty pores (or voids) with side-length of 6.52 nm and periodicity of 13.03 nm. We consider both aligned and staggered distributions of pores. These ordered porous media, with porosity of 12.5%, are small enough to be efficiently simulated via molecular dynamics (MD). Therefore, for benchmarking purposes, we also perform non-equilibrium MD simulations assuming the empirical Stillinger-Webber potential⁷⁹. We consider a computational domain consisting of three periodic unit cells between Langevin thermostats at 310 K and 290 K, respectively. Thus, the total length of the phononic crystals is 39.1 nm. Periodic boundary conditions are imposed along the orthogonal directions to the thermal gradient. After thermalizing the system at room temperature, the steady-state is reached by running the simulation for 1 ns with a time step of 0.5 fs. Thereafter, the local heat flux and apparent conductivity are averaged over the subsequent 4 ns using the same time step size. Further details on the implementation of these MD simulations can be found elsewhere¹².

In Fig. 2, we present steady-state heat flux profiles in the phononic crystal according to the ballistic and hydrodynamic implementations described in Box 1 and Box 2, respectively, along with MD simulations and the diffusive solutions based on Fourier's law. A linear temperature decay across the system is assumed in the ballistic calculation. First, we note that the nanoscale models accommodate non-uniform heat flux profiles between pores, in contrast to the diffusive prediction. At this large Knudsen, however, the shape of the flux profile according to the hydrodynamic model with ab initio values for the parameters in Eq. (4)²⁸ dramatically fails to reproduce MD⁶⁷. Instead, ℓ , C , and κ_{GK} have been modified to match the MD result in Fig. 2. In contrast, the ballistic prediction uses ab initio inputs. This point emphasizes the necessity of reconciling the microscopic phonon properties and the hydrodynamic interpretation at large Knudsen¹².

The heat flux distribution predicted by the ballistic model qualitatively deviates from the MD solution, while the fitted hydrodynamic model provides a reasonably good match throughout the system. Since the geometry under consideration has characteristic length scales smaller than the majority of phonon mean free paths in bulk silicon, the ballistic model does not predict significant internal scattering. Therefore, the behavior of phonons is analogous to photons, and features such as ray-like propagation and shadowing behind the pores emerge. This is in line with previous interpretations in the highly confined limit^{9,10,80}. In contrast, Eq. (4) predicts a fluid-like accommodation of the phonon flow to the system geometry, corresponding to symmetric heat flux patterns relative to the pore symmetry planes and quadratic heat flux profiles along the interpore cross-sections. Microscopically, this is a consequence of the collective diffusion of momentum embodied in the hydrodynamic model, which is absent in the ballistic description due to the lack of scattering. Remarkably, this collective phonon evolution seems necessary to fully describe the MD predictions at the local level of description, thus highlighting the necessity of revising the ballistic assumption under the influence of confinement. More specifically, the ballistic transfer of energy between boundaries by the large fraction of phonons with bulk mean free path much larger than the interpore distance

(cf. Fig. 1a) does not manifest in the atomistic simulations. This inconsistency may be associated with the use of bulk phonon properties to describe ballistic transport in such confined environments, where the phonon dispersion and the phonon-phonon scattering landscape may be altered.

Although the discrepancies between the ballistic and hydrodynamic models are evident in Fig. 2, the global apparent conductivity κ obtained from the different models can be reconciled with experiments^{9,10,12}. Nevertheless, the different phonon dynamics can potentially lead to different global thermal responses. For example, according to the ballistic model, staggered pores block the transfer of energy across the system along the extended channels present in the aligned case, resulting in 9% increase on apparent conductivity κ in the aligned geometry relative to the staggered one in Fig. 2. In contrast, the influence of the pore distribution is less significant in MD or the hydrodynamic fit, which respectively indicate an increase on κ of 5.1% and 5.2% in the aligned geometry. The fitted hydrodynamic scale ℓ is smaller than the interpore distances and, hence, long-range correlations of the flux patterns are not predicted. This attenuates geometric effects unlike the RTA picture where phonons can ballistically travel long distances (cf. Fig. 2). According to the hydrodynamic Eq. (4), the reduction of κ in the staggered case is associated with viscous effects limiting the energy transfer rate due to the enhanced curvature of the flux streamlines (i.e., regions displaying larger $\ell^2 \nabla^2 \mathbf{q}$). Finally, the diffusive description is dominated by the volume reduction effect on κ , thus it predicts nearly identical conductivities for both geometries where the aligned case is only 1.4% higher.

Both the hydrodynamic and ballistic interpretations are based on the particle-like picture of phonons, and any coherent effects potentially arising due to phonon interference in the periodic system are neglected. According to the results in Fig. 2, incorporating these phenomena does not seem key to describing the MD results, which in principle include both the particle-like and wave-like behavior of phonons. However, integration of coherent effects in the ballistic picture has been shown to be relevant in describing the global thermal conductivity in experiments in this particular system by introducing the notion of the Rayleigh ballistic length¹⁰.

Finally, we note that the comparison between models can be extended to a variety of nanostructures and non-equilibrium situations of interest. For example, nanowires have been extensively investigated using both hydrodynamic^{81,82} and ballistic^{83,84} approaches. Another relevant case of study is the heat evacuation process from nanoscale heat sources on semiconductor substrates^{7,32}.

Open challenges

Opportunities remain to advance our understanding of the BTE for modeling heat transport and fully reconcile the different approaches from first principles. On the one hand, while the ballistic approach has been shown to be useful in estimating the apparent global conductivity in semiconductor nanostructures, its underlying assumptions should be revised to capture the local thermal response such as the heat flux distribution in highly confined systems. On the other hand, the ab initio predictive power of hydrodynamic theory has been shown to be limited to $\text{Kn} \leq 1$. Generalizing the moment method to larger Knudsen is thus an outstanding challenge of remarkable fundamental and technological relevance. To this end, comparison with classical MD simulations, as illustrated in the previous section, or fully quantum descriptions such as the nonequilibrium Green's function method^{85,86}, represent a promising route.

Interestingly, these efforts to reconcile, or distinguish, the ballistic interpretation and the emergence of collective, hydrodynamic effects in nanoscale phonon transport are reminiscent of recent advances in modeling electron transport^{87,88}. Electron hydrodynamics has been predicted and predominantly observed in materials where electron-electron interactions, which conserve momentum, are much more frequent than the momentum-relaxing collisions with impurities and boundaries^{89–91}. This notion of electron hydrodynamics, usually demonstrated using bulk resistance measurements, is analogous to phonon hydrodynamics in two-dimensional materials at low temperatures, where normal (momentum-conserving)

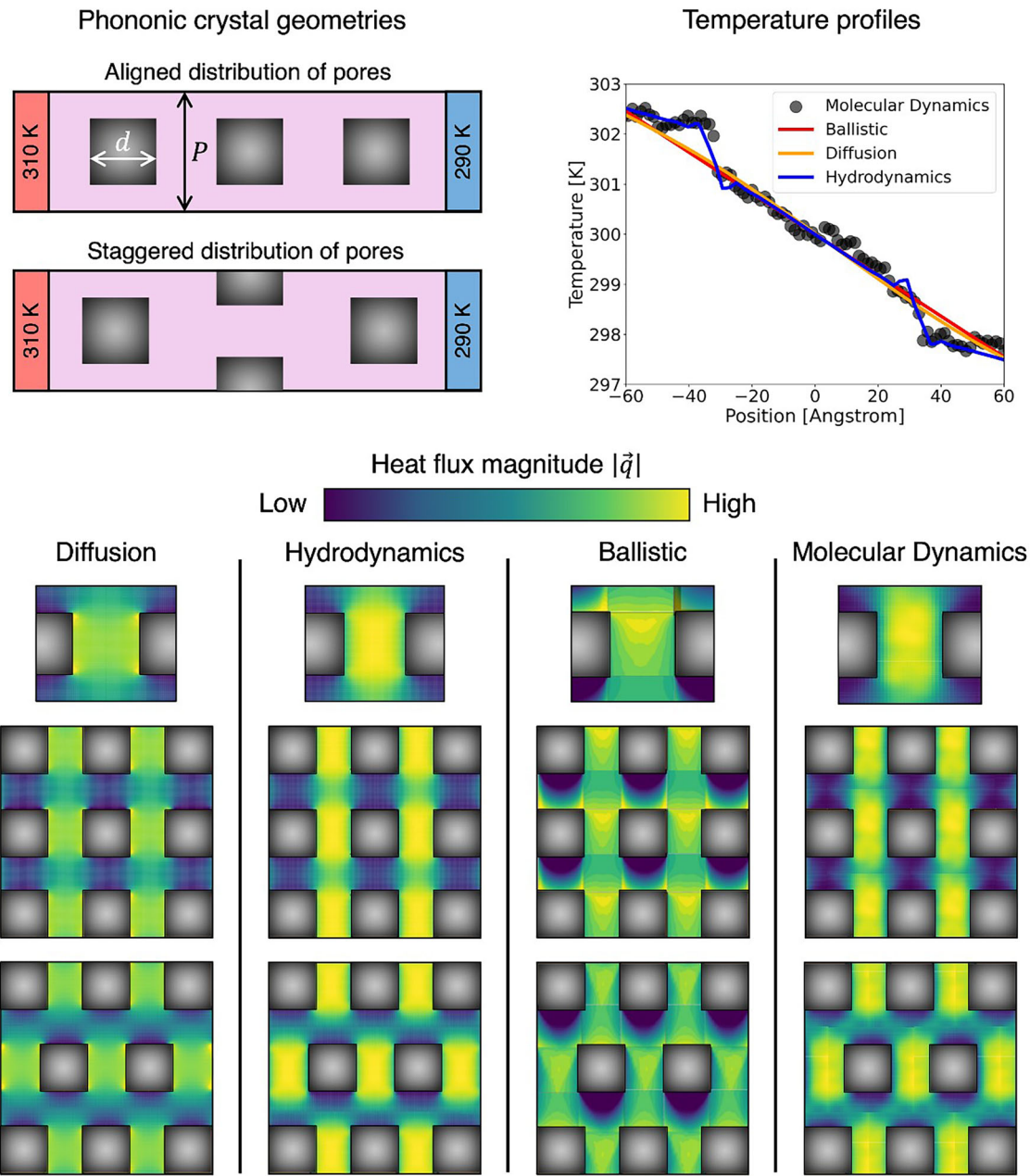


Fig. 2 | Thermal transport in three-dimensional phononic crystals. Top-left: Aligned and Staggered geometries ($d = 6.52 \text{ nm}$ and $P = 13.03 \text{ nm}$). Top-right: Comparison of the temperature profile along the central periodic unit cell of the aligned metalattice. Bottom: Diffusive, hydrodynamic, ballistic, and MD predictions of the normalized heat flux distributions in phononic crystals with aligned and

staggered distributions of pores. The MD predictions of the apparent conductivity κ are $21.6 \text{ W}/(\text{m} \cdot \text{K})$ and $20.55 \text{ W}/(\text{m} \cdot \text{K})$ for the aligned and staggered cases, respectively. The hydrodynamic model uses fitted parameter values to reproduce κ and the flux profiles from MD: $\kappa_{\text{GK}} = 48 \text{ W}/(\text{m} \cdot \text{K})$, $\ell = 0.9 \text{ nm}$, and $C = 0.6$.

collisions are abundant^{52,53}. Notably, hydrodynamic electron signatures in nanostructured systems, such as electron vortices, have also been identified at ultralow temperatures, where momentum-conserving electron interactions are infrequent⁹². This hydrodynamic flow^{93–95} is analogous to the phenomenology discussed in this perspective, which does not require strong normal scattering and thus can emerge in materials such as silicon. However, electrons and phonons exhibit fundamental differences. For example, since phonons are bosons, they are not restricted to a given Fermi volume. Since the BTE for electrons can be characterized by a single scattering time (representative of the carriers close to the Fermi surface), multiscale mean free path spectra are not predicted by the RTA. These differences prevent straightforward extrapolation of electron transport theories to phonons.

Nonetheless, establishing further connections between the kinetic and mesoscopic interpretations of phonon and electron transport would be a promising avenue to develop new charge and heat manipulation strategies.

The theoretical description of electron transport in nanosystems is significantly more advanced than that of phonons, in part due to the availability of complementary experimental techniques for measuring, imaging, and manipulating electrical current⁸⁸, such as nanoscale magnetometry^{92,96–98}. For phonon transport, many experimental capabilities are limited to only indirect measurements of temperature, rather than imaging local heat currents: most techniques monitor the thermal response by measuring a related manifestation such as optical reflectivity or dielectric constant^{4,39,99–102}, lattice expansion¹⁰³, or electrical resistivity^{99,104–106}. In

addition, experiments are typically interpreted employing an effective-diffusion model to extract an apparent thermal conductivity, which is then compared to more advanced models^{10,32,107}. Unfortunately, analyzing raw experimental data through the lens of diffusion masks the underlying microscopic physics⁷; thus, competing theories of thermal transport are validated only at a global level, leading to a plethora of interpretations for similar thermal behaviors despite widely varying microscopic foundations, as is demonstrated in Figs. 1 and 2. Finally, while techniques such as Raman thermometry¹⁰² and ultrafast X-ray scattering¹⁰⁸ can probe single phonon modes, they are often limited in either time or space resolution and do not capture the collective phonon behavior.

These challenges illustrate the compelling need for experimental thermal measurement techniques that can directly map phonon transport in complex three-dimensional geometries with nanoscale spatial resolution and picosecond temporal resolution. In addition, measurement tools agnostic of a particular transport model, *i.e.*, which do not require a layer of effective diffusive modeling, are indispensable to distinguish the underlying phonon physics around the key questions formulated in this perspective, such as the intrinsic phonon length scales that manifest under confinement.

Data availability

Data is provided within the manuscript file.

Received: 4 November 2024; Accepted: 1 April 2025;

Published online: 07 June 2025

References

- Warzoha, R. J. et al. Applications and impacts of nanoscale thermal transport in electronics packaging. *J. Electron. Packag. Trans. ASME* **143**, 020804 (2021).
- Choi, S., Heller, E. R., Dorsey, D., Vetary, R. & Graham, S. The impact of bias conditions on self-heating in AlGaN/GaN HEMTs. *IEEE Trans. Electron Devices* **60**, 159–162 (2013).
- Waldrop, M. M. The chips are down for Moore’s law. *Nat. N.* **530**, 144 (2016).
- Johnson, J. A. et al. Direct measurement of room-temperature nondiffusive thermal transport over micron distances in a silicon membrane. *Phys. Rev. Lett.* **110**, 025901 (2013).
- Benenti, G., Donadio, D., Lepri, S. & Livi, R. Non-Fourier heat transport in nanosystems. *La Riv. del. Nuovo Cim.* **46**, 105–161 (2023).
- Wilson, R. & Cahill, D. G. Anisotropic failure of Fourier theory in time-domain thermoreflectance experiments. *Nat. Commun.* **5**, 5075 (2014).
- Beardo, A. et al. A general and predictive understanding of thermal transport from 1D- and 2D-confined nanostructures: theory and experiment. *ACS Nano* **15**, 13019–13030 (2021).
- Casimir, H. B. G. Note on the conduction of heat in crystals. *Physica* **5**, 495–500 (1938).
- Anufriev, R., Ramiere, A., Maire, J. & Nomura, M. Heat guiding and focusing using ballistic phonon transport in phononic nanostructures. *Nat. Commun.* **8**, 15505 (2017).
- Chen, W. et al. Achieving minimal heat conductivity by ballistic confinement in phononic metalattices. *ACS Nano* **14**, 4235–4243 (2020).
- Guo, Y. & Wang, M. Phonon hydrodynamics for nanoscale heat transport at ordinary temperatures. *Phys. Rev. B* **97**, 035421 (2018).
- McBennett, B. et al. Universal behavior of highly confined heat flow in semiconductor nanosystems: from nanomeshes to metalattices. *Nano Lett.* **23**, 2129–2136 (2023).
- Luckyanova, M. N. et al. Coherent phonon heat conduction in superlattices. *Science* **338**, 936–939 (2012).
- Hussein, M. I., Tsai, C.-N. & Honarvar, H. Thermal conductivity reduction in a nanophononic metamaterial versus a nanophononic crystal: a review and comparative analysis. *Adv. Funct. Mater.* **30**, 1906718 (2020).
- Debernardi, A., Baroni, S. & Molinari, E. Anharmonic phonon lifetimes in semiconductors from density-functional perturbation theory. *Phys. Rev. Lett.* **75**, 1819–1822 (1995).
- Lindsay, L., Hua, C., Ruan, X. & Lee, S. Survey of ab initio phonon thermal transport. *Mater. Today Phys.* **7**, 106–120 (2018).
- Broido, D. A., Malorny, M., Birner, G., Mingo, N. & Stewart, D. A. Intrinsic lattice thermal conductivity of semiconductors from first principles. *Appl. Phys. Lett.* **91**, 231922 (2007).
- Esfarjani, K., Chen, G. & Stokes, H. T. Heat transport in silicon from first-principles calculations. *Phys. Rev. B* **84**, 085204 (2011).
- Cepellotti, A. & Marzari, N. Thermal transport in crystals as a kinetic theory of relaxons. *Phys. Rev. X* **6**, 041013 (2016).
- Chiloyan, V. et al. Green’s functions of the Boltzmann transport equation with the full scattering matrix for phonon nanoscale transport beyond the relaxation-time approximation. *Phys. Rev. B* **104**, 245424 (2021).
- Jeong, J., Li, X., Lee, S., Shi, L. & Wang, Y. Transient hydrodynamic lattice cooling by picosecond laser irradiation of graphite. *Phys. Rev. Lett.* **127**, 085901 (2021).
- Chen, G. Ballistic-diffusive heat-conduction equations. *Phys. Rev. Lett.* **86**, 2297–2300 (2001).
- Lacroix, D., Joulain, K. & Lemonnier, D. Monte Carlo transient phonon transport in silicon and germanium at nanoscales. *Phys. Rev. B* **72**, 064305 (2005).
- Maznev, A. A., Johnson, J. A. & Nelson, K. A. Onset of nondiffusive phonon transport in transient thermal grating decay. *Phys. Rev. B* **84**, 195206 (2011).
- Hua, C., Lindsay, L., Chen, X. & Minnich, A. J. Generalized Fourier’s law for nondiffusive thermal transport: theory and experiment. *Phys. Rev. B* **100**, 085203 (2019).
- Struchtrup, H. *Macroscopic transport equations for rarefied gas flows* (Springer, 2005).
- Simoncelli, M., Marzari, N. & Cepellotti, A. Generalization of Fourier’s law into viscous heat equations. *Phys. Rev. X* **10**, 011019 (2020).
- Sendra, L. et al. Derivation of a hydrodynamic heat equation from the phonon Boltzmann equation for general semiconductors. *Phys. Rev. B* **103**, L140301 (2021).
- Jou, D., Casas-Vázquez, J. & Lebon, G. *Extended irreversible thermodynamics* (Springer, 1996).
- Kovács, R. Heat equations beyond Fourier: from heat waves to thermal metamaterials. *Phys. Rep.* **1048**, 1–75 (2024).
- Ziman, J. M. Electrons and phonons: the theory of transport phenomena in solids (2001).
- Hu, Y., Zeng, L., Minnich, A. J., Dresselhaus, M. S. & Chen, G. Spectral mapping of thermal conductivity through nanoscale ballistic transport. *Nat. Nanotechnol.* **10**, 701–706 (2015).
- Guo, Y. & Wang, M. Heat transport in two-dimensional materials by directly solving the phonon Boltzmann equation under Callaway’s dual relaxation model. *Phys. Rev. B* **96**, 134312 (2017).
- Zhang, C. & Guo, Z. Discrete unified gas kinetic scheme for multiscale heat transfer with arbitrary temperature difference. *Int. J. Heat. Mass Transf.* **134**, 1127–1136 (2019).
- Péraud, J.-P. M. & Hadjiconstantinou, N. G. Efficient simulation of multidimensional phonon transport using energy-based variance-reduced Monte Carlo formulations. *Phys. Rev. B* **84**, 205331 (2011).
- Ran, X., Huang, Y. & Wang, M. A hybrid Monte Carlo-discrete ordinates method for phonon transport in micro/nanosystems with rough interfaces. *Int. J. Heat. Mass Transf.* **201**, 123624 (2023).
- Minnich, A. J. et al. Thermal conductivity spectroscopy technique to measure phonon mean free paths. *Phys. Rev. Lett.* **107**, 095901 (2011).

38. Vermeersch, B., Carrete, J., Mingo, N. & Shakouri, A. Superdiffusive heat conduction in semiconductor alloys. I. Theoretical foundations. *Phys. Rev. B* **91**, 085202 (2015).
39. Cuffe, J. et al. Reconstructing phonon mean-free-path contributions to thermal conductivity using nanoscale membranes. *Phys. Rev. B* **91**, 245423 (2015).
40. Guyer, R. A. & Krumhansl, J. A. Solution of the linearized phonon Boltzmann equation. *Phys. Rev.* **148**, 766–778 (1966).
41. Guo, Y., Jou, D. & Wang, M. Nonequilibrium thermodynamics of phonon hydrodynamic model for nanoscale heat transport. *Phys. Rev. B* **98**, 104304 (2018).
42. Tzou, D. Y. *Macro-to microscale heat transfer: the lagging behavior* (John Wiley & Sons, 2014).
43. Rieth, Á., Kovács, R. & Fülöp, T. Implicit numerical schemes for generalized heat conduction equations. *Int. J. Heat. Mass Transf.* **126**, 1177–1182 (2018).
44. Beardo, A. et al. Hydrodynamic heat transport in compact and holey silicon thin films. *Phys. Rev. Appl.* **11**, 034003 (2019).
45. Beardo, A. et al. Hydrodynamic thermal transport in silicon at temperatures ranging from 100 to 300 K. *Phys. Rev. B* **105**, 165303 (2022).
46. Xiang, Z., Jiang, P. & Yang, R. Time-domain thermoreflectance (TDTR) data analysis using phonon hydrodynamic model. *J. Appl. Phys.* **132**, 205104 (2022).
47. Kovács, R. Analytic solution of Guyer-Krumhansl equation for laser flash experiments. *Int. J. Heat. Mass Transf.* **127**, 631–636 (2018).
48. Beardo, A. et al. Phonon hydrodynamics in frequency-domain thermoreflectance experiments. *Phys. Rev. B* **101**, 075303 (2020).
49. Sussmann, J. & Thellung, A. Thermal conductivity of perfect dielectric crystals in the absence of umklapp processes. *Proc. Phys. Soc.* **81**, 1122 (1963).
50. Hardy, R. J. & Albers, D. L. Hydrodynamic approximation to the phonon Boltzmann equation. *Phys. Rev. B* **10**, 3546 (1974).
51. Beck, H., Meier, P. F. & Thellung, A. Phonon hydrodynamics in solids. *Phys. Status Solidi (a)* **24**, 11–63 (1974).
52. Cepellotti, A. et al. Phonon hydrodynamics in two-dimensional materials. *Nat. Commun.* **6**, 6400 (2015).
53. Lee, S., Broido, D., Esfarjani, K. & Chen, G. Hydrodynamic phonon transport in suspended graphene. *Nat. Commun.* **6**, 6290 (2015).
54. Jackson, H. E., Walker, C. T. & McNelly, T. F. Second sound in NaF. *Phys. Rev. Lett.* **25**, 26–28 (1970).
55. Huberman, S. et al. Observation of second sound in graphite at temperatures above 100 K. *Science* **364**, 375–379 (2019).
56. Han, Z. & Ruan, X. Thermal conductivity of monolayer graphene: convergent and lower than diamond. *Phys. Rev. B* **108**, L121412 (2023).
57. Sellitto, A., Carlomagno, I. & Jou, D. Two-dimensional phonon hydrodynamics in narrow strips. *Proc. R. Soc. A Math. Phys. Eng. Sci.* **471**, 20150376 (2015).
58. Tur-Prats, J. et al. Microscopic origin of heat vorticity in quasi-ballistic phonon transport. *Int. J. Heat. Mass Transf.* **226**, 125464 (2024).
59. Vermeersch, B., Mohammed, A. M. S., Pernot, G., Koh, Y. R. & Shakouri, A. Superdiffusive heat conduction in semiconductor alloys. II. Truncated Lévy formalism for experimental analysis. *Phys. Rev. B* **91**, 085203 (2015).
60. Huberman, S. et al. Unifying first-principles theoretical predictions and experimental measurements of size effects in thermal transport in SiGe alloys. *Phys. Rev. Mater.* **1**, 054601 (2017).
61. Zenji, A. et al. Seeking non-Fourier heat transfer with ultrabroad band thermoreflectance spectroscopy. *Commun. Mater.* **5**, 123 (2024).
62. Holland, M. G. Analysis of lattice thermal conductivity. *Phys. Rev.* **132**, 2461–2471 (1963).
63. Marconnet, A. M., Asheghi, M. & Goodson, K. E. From the Casimir limit to phononic crystals: 20 years of phonon transport studies using silicon-on-insulator technology. *J. Heat. Transf.* **135**, 061601 (2013).
64. Verdier, M., Anufriev, R., Ramiere, A., Termentzidis, K. & Lacroix, D. Thermal conductivity of phononic membranes with aligned and staggered lattices of holes at room and low temperatures. *Phys. Rev. B* **95**, 205438 (2017).
65. Alvarez, F. X. & Jou, D. Memory and nonlocal effects in heat transport: from diffusive to ballistic regimes. *Appl. Phys. Lett.* **90**, 083109 (2007).
66. Sciacca, M. & Jou, D. A power-law model for nonlinear phonon hydrodynamics. *Z. f. ür. Angew. Mathematik und Phys.* **75**, 70 (2024).
67. Desmarchelier, P., Beardo, A., Alvarez, F. X., Tanguy, A. & Termentzidis, K. Atomistic evidence of hydrodynamic heat transfer in nanowires. *Int. J. Heat. Mass Transf.* **194**, 123003 (2022).
68. Bhatnagar, P. L., Gross, E. P. & Krook, M. A model for collision processes in gases. I. Small amplitude processes in charged and neutral one-component systems. *Phys. Rev.* **94**, 511 (1954).
69. Callaway, J. Model for lattice thermal conductivity at low temperatures. *Phys. Rev.* **113**, 1046–1051 (1959).
70. Jain, A., Yu, Y.-J. & McGaughey, A. J. H. Phonon transport in periodic silicon nanoporous films with feature sizes greater than 100 nm. *Phys. Rev. B* **87**, 195301 (2013).
71. Takahashi, K. et al. Elastic inhomogeneity and anomalous thermal transport in ultrafine Si phononic crystals. *Nano Energy* **71**, 104581 (2020).
72. Asheghi, M., Touzelbaev, M. N., Goodson, K. E., Leung, Y. K. & Wong, S. S. Temperature-dependent thermal conductivity of single-crystal silicon layers in SOI substrates. *J. Heat. Transf.* **120**, 30–36 (1998).
73. Ju, Y. S. & Goodson, K. E. Phonon scattering in silicon films with thickness of order 100 nm. *Appl. Phys. Lett.* **74**, 3005–3007 (1999).
74. Hao, Z. et al. Thermal conductivity measurements of ultra-thin single crystal silicon films using improved structure. In *2006 8th International Conference on Solid-State and Integrated Circuit Technology Proceedings*, 2196–2198 (IEEE, 2006).
75. Liu, W. & Asheghi, M. Thermal conductivity measurements of ultra-thin single crystal silicon layers. *J. Heat. Transf.* **128**, 75–83 (2005).
76. Aubain, M. S. & Bandaru, P. R. Determination of diminished thermal conductivity in silicon thin films using scanning thermoreflectance thermometry. *Appl. Phys. Lett.* **97**, 253102 (2010).
77. Aubain, M. S. & Bandaru, P. R. In-plane thermal conductivity determination through thermoreflectance analysis and measurements. *J. Appl. Phys.* **110**, 084313 (2011).
78. Chávez-Ángel, E. et al. Reduction of the thermal conductivity in free-standing silicon nano-membranes investigated by non-invasive Raman thermometry. *APL Mater.* **2**, 012113 (2014).
79. Stillinger, F. H. & Weber, T. A. Computer simulation of local order in condensed phases of silicon. *Phys. Rev. B* **31**, 5262–5271 (1985).
80. Schleeh, J. et al. Phonon black-body radiation limit for heat dissipation in electronics. *Nat. Mater.* **14**, 187–192 (2015).
81. Alvarez, F. X., Jou, D. & Sellitto, A. Phonon hydrodynamics and phonon-boundary scattering in nanosystems. *J. Appl. Phys.* **105**, 014317 (2009).
82. Rezgui, H. et al. Nanoscale thermal transport in vertical gate-all-around junctionless nanowire transistors—Part II: Multiphysics simulation. *IEEE Transactions on Electron Devices* (2023).
83. Lacroix, D., Joulain, K., Terris, D. & Lemonnier, D. Monte Carlo simulation of phonon confinement in silicon nanostructures: application to the determination of the thermal conductivity of silicon nanowires. *Appl. Phys. Lett.* **89**, 103104 (2006).
84. Anufriev, R., Gluchko, S., Volz, S. & Nomura, M. Quasi-ballistic heat conduction due to Lévy phonon flights in silicon nanowires. *ACS Nano* **12**, 11928–11935 (2018).
85. Yamamoto, T. & Watanabe, K. Nonequilibrium Green's function approach to phonon transport in defective carbon nanotubes. *Phys. Rev. Lett.* **96**, 255503 (2006).
86. Chen, Y.-J. & Lü, J.-T. Local heat current flow in ballistic phonon transport of graphene nanoribbons. *Phys. Rev. B* **110**, 035422 (2024).

87. Qi, M. & Lucas, A. Distinguishing viscous, ballistic, and diffusive current flows in anisotropic metals. *Phys. Rev. B* **104**, 195106 (2021).
88. Varnavides, G., Yacoby, A., Felser, C. & Narang, P. Charge transport and hydrodynamics in materials. *Nat. Rev. Mater.* **8**, 1–16 (2023).
89. Crossno, J. et al. Observation of the Dirac fluid and the breakdown of the Wiedemann-Franz law in graphene. *Science* **351**, 1058–1061 (2016).
90. Moll, P. J., Kushwaha, P., Nandi, N., Schmidt, B. & Mackenzie, A. P. Evidence for hydrodynamic electron flow in PdCoO₂. *Science* **351**, 1061–1064 (2016).
91. Bandurin, D. A. et al. Negative local resistance caused by viscous electron backflow in graphene. *Science* **351**, 1055–1058 (2016).
92. Aharon-Steinberg, A. et al. Direct observation of vortices in an electron fluid. *Nature* **607**, 74–80 (2022).
93. Gupta, A. et al. Hydrodynamic and ballistic transport over large length scales in GaAs/AlGaAs. *Phys. Rev. Lett.* **126**, 076803 (2021).
94. Wolf, Y., Aharon-Steinberg, A., Yan, B. & Holder, T. Para-hydrodynamics from weak surface scattering in ultraclean thin flakes. *Nat. Commun.* **14**, 2334 (2023).
95. Estrada-Álvarez, J., Domínguez-Adame, F. & Díaz, E. Alternative routes to electron hydrodynamics. *Commun. Phys.* **7**, 138 (2024).
96. Palm, M. L. et al. Observation of current whirlpools in graphene at room temperature. *Science* **384**, 465–469 (2024).
97. Ku, M. J. H. et al. Imaging viscous flow of the Dirac fluid in graphene. *Nature* **583**, 537–541 (2020).
98. Vasyukov, D. et al. A scanning superconducting quantum interference device with single electron spin sensitivity. *Nat. Nanotechnol.* **8**, 639–644 (2013).
99. Cahill, D. G. et al. Nanoscale thermal transport. II. 2003–2012. *Appl. Phys. Rev.* **1**, 011305 (2014).
100. Koh, Y. K. & Cahill, D. G. Frequency dependence of the thermal conductivity of semiconductor alloys. *Phys. Rev. B* **76**, 075207 (2007).
101. Regner, K. T. et al. Broadband phonon mean free path contributions to thermal conductivity measured using frequency domain thermoreflectance. *Nat. Commun.* **4**, 1640–1647 (2013).
102. Liu, J., Han, M., Wang, R., Xu, S. & Wang, X. Photothermal phenomenon: extended ideas for thermophysical properties characterization. *J. Appl. Phys.* **131**, 065107 (2022).
103. Frazer, T. D. et al. Engineering nanoscale thermal transport: size- and spacing-dependent cooling of nanostructures. *Phys. Rev. Appl.* **11**, 024042 (2019).
104. Dames, C. Measuring the thermal conductivity of thin films: 3 omega and related electrothermal methods. *Annu. Rev. Heat. Transf.* **16**, 7–49 (2013).
105. Kim, P., Shi, L., Majumdar, A. & McEuen, P. L. Thermal transport measurements of individual multiwalled nanotubes. *Phys. Rev. Lett.* **87**, 215502 (2001).
106. Majumdar, A. Scanning thermal microscopy. *Annu. Rev. Mater. Res.* **29**, 505–585 (1999).
107. Yang, J., Maragliano, C. & Schmidt, A. J. Thermal property microscopy with frequency domain thermoreflectance. *Rev. Sci. Instrum.* **84**, 104904 (2013).
108. Trigo, M. et al. Fourier-transform inelastic X-ray scattering from time- and momentum-dependent phonon–phonon correlations. *Nat. Phys.* **9**, 790–794 (2013).

Acknowledgements

The authors acknowledge support from the STROBE National Science Foundation Science & Technology Center, Grant No. DMR-1548924. A.B. acknowledges support from the Spanish Ministerio de Ciencia, Innovación y Universidades, Grant No. PID2021-122322NB-I00 and TED2021-129612B-C22 (MCIU/AEI/10.13039/501100011033/FEDER UE) and the AGAUR - Generalitat de Catalunya, Grant No. 2021-SGR-00644. This work utilized the Alpine high performance computing resource at the University of Colorado Boulder. Alpine is jointly funded by the University of Colorado Boulder, the University of Colorado Anschutz, and Colorado State University. T.K.S. and I.D. acknowledge primarily support from the Center for Nanoscale Science under Grants No. DMR-1420620 and No. DMR-2011839 [NSF-funded Materials Research Science and Engineering Centers (MRSEC)].

Author contributions

A.B., B.M., J.K., M.M., and I.D. wrote the manuscript. A.B. performed the molecular dynamics simulations and the calculations based on the hydrodynamic model. W.C. performed the calculations based on the ballistic model. A.B., T.S., J.K., I.D. prepared the Figures. M.M. and I.D. supervised the project. All authors participated in the discussion and reviewed the manuscript.

Competing interests

The authors declare no competing interests.

Additional information

Correspondence and requests for materials should be addressed to Albert Beardo.

Reprints and permissions information is available at <http://www.nature.com/reprints>

Publisher's note Springer Nature remains neutral with regard to jurisdictional claims in published maps and institutional affiliations.

Open Access This article is licensed under a Creative Commons Attribution-NonCommercial-NoDerivatives 4.0 International License, which permits any non-commercial use, sharing, distribution and reproduction in any medium or format, as long as you give appropriate credit to the original author(s) and the source, provide a link to the Creative Commons licence, and indicate if you modified the licensed material. You do not have permission under this licence to share adapted material derived from this article or parts of it. The images or other third party material in this article are included in the article's Creative Commons licence, unless indicated otherwise in a credit line to the material. If material is not included in the article's Creative Commons licence and your intended use is not permitted by statutory regulation or exceeds the permitted use, you will need to obtain permission directly from the copyright holder. To view a copy of this licence, visit <http://creativecommons.org/licenses/by-nc-nd/4.0/>.

© The Author(s) 2025